symmetry

MDPI

Article

Molecular Dynamics Simulations of CeO_2 Nano-Fuel: Thermodynamic and Kinetic Properties

Rui Zhang [1,2], Jianbo Zhou [3], Yingjie Zhao [1], Zhen He [1], Wenxiong Xi [2] and Weidong Zhao [4,*]

[1] School of Engineering Science, Shandong Xiehe University, Jinan 250107, China; zhangrui@sdxiehe.edu.cn (R.Z.); zhaoyingjie@sdxiehe.edu.cn (Y.Z.); hezhen@sdxiehe.edu.cn (Z.H.)
[2] School of Aeronautics and Astronautics, Central South University, Changsha 410073, China; 13739076081@163.com
[3] School of Aeronautical Electromechanical Equipment Maintenance, Airforce Aviation Repair Institute of Technology, Changsha 410073, China; nchu_zhou@163.com
[4] School of Automotive and Traffic Engineering, Jiangsu University, Zhenjiang 212013, China
* Correspondence: zhaowd@ujs.edu.cn

Abstract: This study explores the thermodynamic and kinetic properties of CeO_2 nano-fuels, with a particular focus on the influence of nanoparticle additives on the diffusion and thermal conductivity of C14-based fuel systems. Using molecular dynamics simulations and the COMPASS force field, we model the interactions between C14 molecules and CeO_2 nanoparticles, varying nanoparticle size and concentration. Our results reveal that the inclusion of CeO_2 nanoparticles leads to significant enhancements in both thermal conductivity (increasing by 9.8–23.6%) and diffusion coefficients (increasing by approximately 140%) within the 20 °C to 100 °C temperature range. These improvements are attributed to the interactions between nanoparticles and fuel molecules, which facilitate more efficient energy and mass transport. Notably, nanoparticles with smaller sizes (0.2 nm and 0.5 nm) exhibit more pronounced effects on both the thermodynamic and kinetic properties than larger nanoparticle analogs (20 nm and 50 nm). The study also highlights the temperature-dependent nature of these properties, demonstrating that nanoparticle additives enhance the fuel's thermal stability and diffusion behavior, particularly at elevated temperatures. This work provides valuable insights into the optimization of nano-fuel systems, with potential applications in enhancing the performance and efficiency of diesel combustion and heat transfer processes.

Keywords: nano-fuel; combustion; thermal properties; molecule dynamics

check for updates

Academic Editor: Luigi Nicolais

Received: 26 January 2025
Revised: 11 February 2025
Accepted: 14 February 2025
Published: 16 February 2025

Citation: Zhang, R.; Zhou, J.; Zhao, Y.; He, Z.; Xi, W.; Zhao, W. Molecular Dynamics Simulations of CeO_2 Nano-Fuel: Thermodynamic and Kinetic Properties. *Symmetry* **2025**, *17*, 296. https://doi.org/10.3390/sym17020296

Copyright: © 2025 by the authors. Licensee MDPI, Basel, Switzerland. This article is an open access article distributed under the terms and conditions of the Creative Commons Attribution (CC BY) license (https://creativecommons.org/licenses/by/4.0/).

1. Introduction

The invention and widespread application of internal combustion engines have profoundly transformed industries such as transportation, power generation, and heavy machinery, driving significant advancements in societal development [1–3]. However, these engines rely heavily on petroleum-based fuels, and their combustion processes release harmful gases that negatively impact atmospheric environments. As a result, conserving nonrenewable energy resources, developing clean energy alternatives, and optimizing energy consumption structures have become critical priorities in the energy sector [4–6].

Current approaches to improving fuel quality predominantly focus on the use of fuel additives and advancements in fuel formulations. Recent studies on fuel additives have highlighted the potential benefits of incorporating nanoscale elemental metals and their oxides into conventional fuels. These nano-additives not only enhance fuel efficiency and

combustion performance but also exhibit high surface reactivity, which facilitates catalytic oxidation and regeneration in diesel particulate filters, thereby significantly reducing pollutant emissions [7–10].

Nanoparticles, due to their diminutive size, are significantly influenced by factors such as particle motion and intermolecular forces. Their effect on the heat transfer processes of base liquid fuels is highly intricate and cannot be fully explained or validated using macroscopic theories or conventional experimental methods. This complexity necessitates the use of simulation-based approaches to better understand how nanoparticles alter the heat and mass transfer characteristics of base fuels. Moreover, the combustion of nano-fuel droplets involves multiphase flow, multiscale dynamics, and multi-component processes—phenomena that exceed the explanatory capacity of macroscopic theories or standard experimental techniques [11–13]. Therefore, a molecular-level analysis is indispensable for a comprehensive understanding of how nano-fuel microstructures influence their heat transfer properties, flow behavior, and ignition characteristics.

For instance, Tian et al. [14] examined the factors influencing the thermal conductivity of Cu/Ar nanofluids and found that thermal conductivity is primarily dependent on particle mass concentration and size rather than shape. Kumar et al. investigated the impact of Brownian motion of Al nanoparticles on the thermal conductivity of base fluids, considering the effects from the perspective of molecular Brownian motion [15]. Similarly, Yang utilized perturbation-based non-equilibrium molecular dynamics to explore diffusion coefficients in the Fe/H_2O system, noting that particle shape had minimal influence on diffusion behavior [16]. Sundar et al. [17] observed that the dynamic viscosity of SiO_2/H_2O nanofluids decreases with increasing temperature above 30 °C, although it remains higher than that of pure water.

Over decades of development, microscopic-scale simulation techniques have become more refined, with molecular dynamics (MD) methods emerging as the primary approach for studying the thermal properties of nanofluids. In this study, we employ the Reverse non-equilibrium molecular dynamics (RNEMD) method to investigate CeO_2-based nano-fuel systems. Using custom Perl scripts, we calculate the dynamic viscosity and thermal conductivity for various CeO_2 nano-fuel configurations. Additionally, by analyzing heat flux, temperature gradients, mean square displacement, diffusion coefficients, and radial distribution functions, we provide a comprehensive exploration of the microscopic mechanisms by which nanoparticle size and mass concentration influence the thermal properties of base liquid fuel.

2. Model Construction and Optimization

Diesel fuel, as a complex hydrocarbon mixture, primarily consists of alkanes, al-kenes, cycloalkanes, and trace amounts of sulfur compounds. The varying proportions of these components directly affect key physicochemical properties such as density, viscosity, and boiling point, making the precise determination of these attributes a significant challenge. These complexities also pose difficulties in subsequent investigations into the thermal properties and ignition behavior of nano-fuels.

In contrast, the C14 molecular model, used as a surrogate for diesel fuel, provides a simplified yet effective approximation of diesel's overall behavior. Despite being a single-component structure, C14 shares similar physicochemical properties with diesel fuel, making it widely used in prior research. Table 1 summarizes the key physical properties of C14, showing a good correspondence with diesel in terms of viscosity, density, and boiling point. This similarity makes C14 an ideal choice for the base liquid in nano-fuel molecular simulations, allowing for a focused investigation of the effects of nanoparticle additives, specifically CeO_2, on fuel performance.

Although the C14 model does not fully replicate the diversity of hydrocarbon components found in diesel fuel, its simplified nature offers significant advantages in studying the interactions between liquid fuel and nanoparticle additives. As a linear alkane, C14 reduces the computational complexity of molecular simulations, enabling a concentrated analysis of interactions between the base fuel and CeO_2 nanoparticles, as depicted in Figures 1 and 2, where the molecular structures of C14 and CeO_2 are shown.

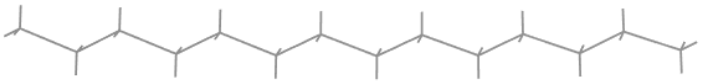


Figure 1. C14 Molecular Structure Model.

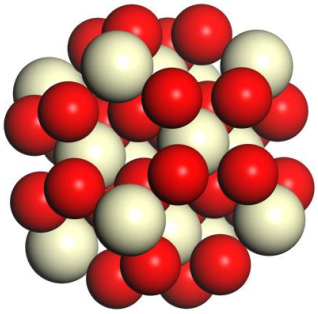


Figure 2. Molecular structure of CeO_2 nanoparticles.

Table 1. Key physical properties of n-Tetradecane.

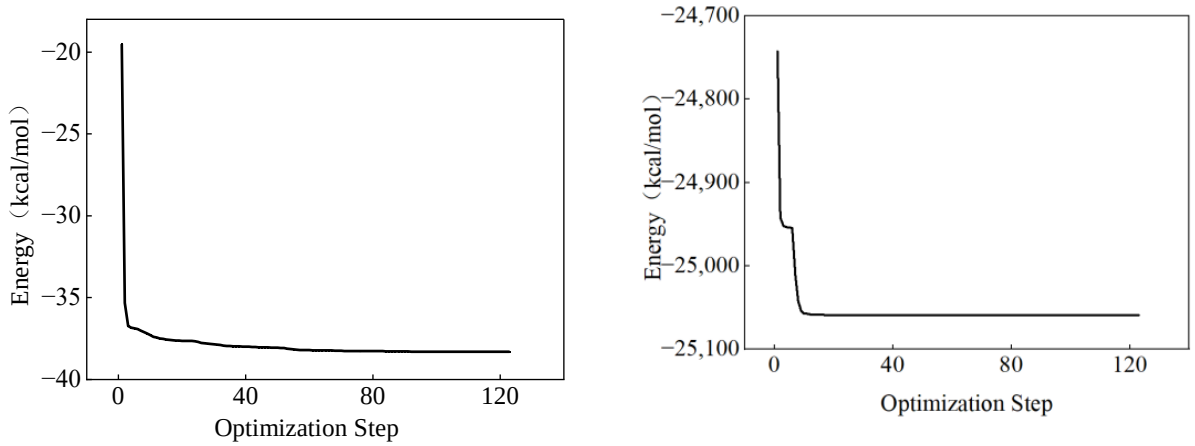
Parameter	Unit	Value
Molar Mass	g/mol	198.39
Standard Boiling Point	°C	253.58
Density	g/cm^3	0.76
Critical Pressure	MPa	1.57

Therefore, while the C14 model cannot completely capture the complexity of the hydrocarbon composition of diesel fuel, its physicochemical properties closely resemble those of diesel, making it a reliable surrogate for studying nano-fuel systems. The use of C14 is justified not only by its similarity in key properties but also by the computational simplicity it offers, thereby facilitating the investigation of nano-fuel behavior, particularly in terms of thermal properties and ignition performance.

Following the construction of the C14 and CeO_2 molecular models, Geometry Optimization was carried out using the Forcite Geometry Optimization module, with a simulation duration of 250 ps. The energy fluctuations during the optimization process are illustrated in Figure 3. The results demonstrate a steady decrease in the structural energy of both molecular models over the course of the calculation, ultimately reaching a stable state. This stabilization confirms the suitability of these models for constructing subsequent nano-fuel molecular systems [18–22].

After optimizing the C14 and CeO_2 molecular models, the Packing module in the Amorphous Cell (AC) was employed to construct the CeO_2 nano-fuel molecular model, with the parameter settings outlined in Figure 4. The convergence accuracy of the model has a significant impact on the computational time. Through a series of simulations, it was determined that setting the convergence precision to "Medium" provided an effective balance between accuracy and computational efficiency. The density of C14 was set to 0.76 g/cm^3, and the CeO_2 molecular model was configured with a fill factor of 1. From the current calculation results, the selection of high precision can slightly optimize the

molecular geometry, reduce the initial potential energy of the system, and improve the accuracy of energy calculation. The calculation of RDF and diffusion coefficients may be slightly improved, with error variations of no more than 2–3%. During computing, it was found that the use of "High" accuracy resulted in a 5–10-fold increase in optimization time, which significantly increased the total amount of computation for simulations involving multiple temperature field calculations. Since this study focuses on the trend of temperature influence on CeO_2 nano-fuel diffusion behavior and heat transfer and does not rely on structural optimization with extremely high precision, the use of "Medium" precision is reasonable. To sum up, the selection of "Medium" accuracy is based on the optimization consideration between calculation time and accuracy. The literature research and test results show that compared with "High" accuracy, the calculation error under "Medium" accuracy is usually within the acceptable range (less than 3%), and the calculation time is significantly reduced, ensuring the feasibility and efficiency of the simulation. Therefore, the accuracy of "Medium" will not significantly affect the reliability of the research conclusions.



(**a**) C14 (**b**) CeO_2

Figure 3. Energy variation during molecular structure optimization.

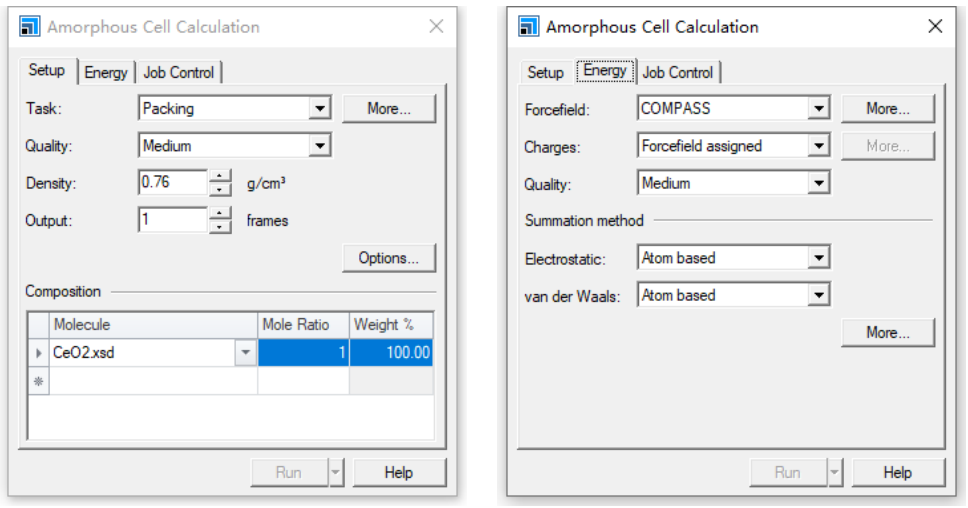


Figure 4. Packing module parameter settings.

The COMPASS force field, specifically developed for organic polymer systems and metal–oxide mixtures, was chosen due to its superior compatibility with the CeO_2 nano-fuel system compared to other available force fields. All subsequent structural optimizations

and thermal property calculations for the CeO_2 nano-fuel system were performed using the COMPASS force field.

Molecular dynamics simulations primarily focus on the microscopic behaviors of atoms and molecules, typically involving relatively small computational systems ranging from 1 nm^3 to 700 nm^3. However, due to the limitations inherent in nanoparticle fabrication techniques, the CeO_2 nanoparticles used in the subsequent ignition experiments possess significantly larger diameters of 20 nm and 50 nm, which far exceed the dimensions of the molecular simulation systems.

To facilitate comparisons of the effects of varying nanoparticle sizes on the thermal properties of fuels, a mass-analogy method was employed. Spherical cluster models with diameters of 0.2 nm and 0.5 nm were constructed to represent 20 nm and 50 nm CeO_2 nanoparticles, respectively. For clarity, the designation Ce_B^A is used to represent different types of nano-fuels, where subscript B indicates particle diameter, and superscript A represents mass concentration (in mg/L). For example, Ce_{50}^{150} denotes a nano-fuel with particle diameters of 50 nm and a concentration of 150 mg/L. The composition and dimensions of different nano-fuel molecular systems are summarized in Table 2.

Table 2. Compositions of nano-fuel molecular model systems.

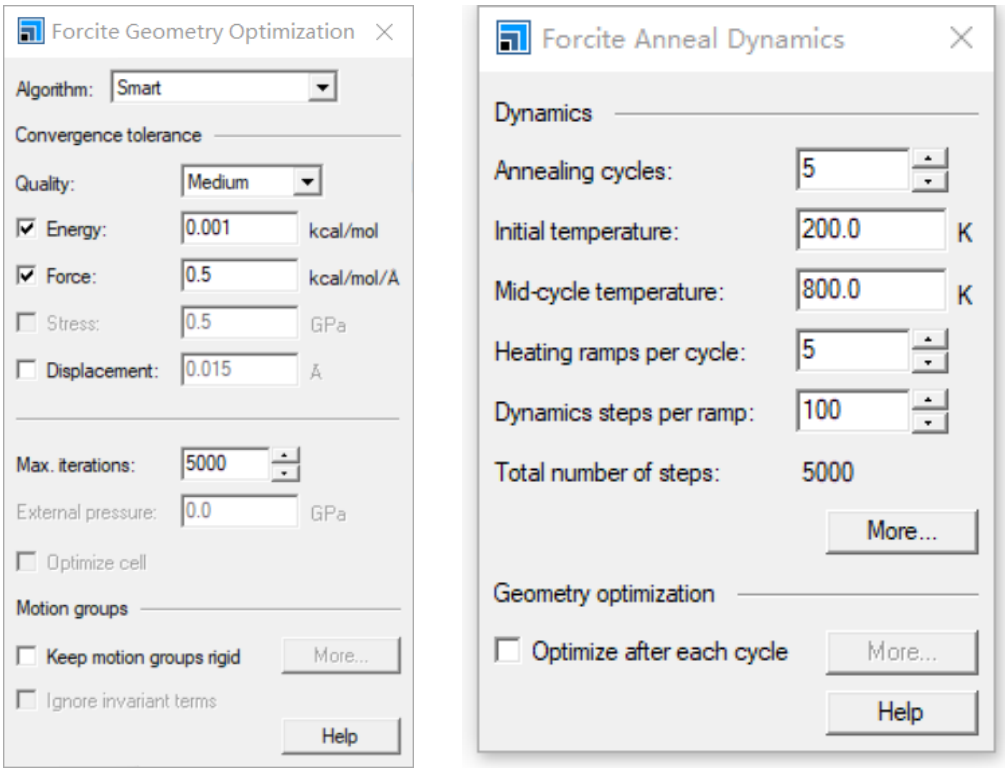
Fuel Type	System Size (Å)	Number of C14 Molecules	Number of CeO_2 Molecules
Ce_{20}^{50}	72	1132	4
Ce_{20}^{100}	57.3	570	4
Ce_{20}^{150}	50	380	4
Ce_{50}^{50}	97.7	2830	10
Ce_{50}^{100}	77.5	1414	10
Ce_{50}^{150}	67.7	942	10

The Packing module in the Amorphous Cell (AC), based on the Monte Carlo method, generates amorphous random models. However, these models may exhibit unrealistic intermolecular distances and excessive system energy, which can significantly impact the accuracy of molecular dynamics simulations [23–25]. Consequently, it is essential to optimize the model structure and minimize system energy before performing molecular dynamics calculations.

To address this, the Geometry Optimization and Anneal modules in Forcite were utilized to refine the molecular configuration and perform annealing, respectively. The Geometry Optimization module improves the molecular structure of the CeO_2 nano-fuel model by alleviating structural stress, while the Anneal module effectively dissipates excess system energy, returning the molecular structure to its ground-state energy [26–30].

The optimization and annealing parameters are detailed in Figure 5. The Geometry Optimization was performed using Forcite, with 5000 calculation steps and a convergence accuracy set to "Medium." The annealing process consisted of five cycles, with initial and intermediate cycle temperatures set to 200 K and 800 K, respectively, and 5000 calculation steps per cycle.

Using Ce_{20}^{50} as an example, five annealing cycles were performed under the COMPASS force field within an NVT (constant number of particles, volume, and temperature) ensemble. The energy variation in the molecular system across the five annealing cycles is shown in Figure 6. The results indicate that annealing effectively dissipates excess system energy, with the molecular configuration achieving its lowest energy state after the fifth cycle. The configuration with the lowest system energy was selected for subsequent molecular dynamics simulations and thermal property analyses [31–33].



(**a**) Structural optimization parameters (**b**) Annealing parameters

Figure 5. Structural optimization and annealing parameter settings.

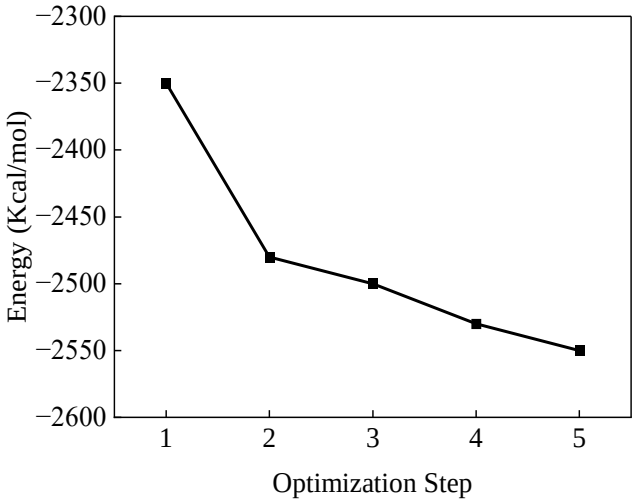


Figure 6. Energy variation of Ce_{20}^{50} during annealing.

The molecular dynamics simulations for CeO_2 nano-fuel were conducted under the NVT ensemble, as detailed in Figure 7. The system temperature was varied from 20 °C to 100 °C, with dynamic information collected at 20 °C intervals. Each simulation was conducted for 250 ps.

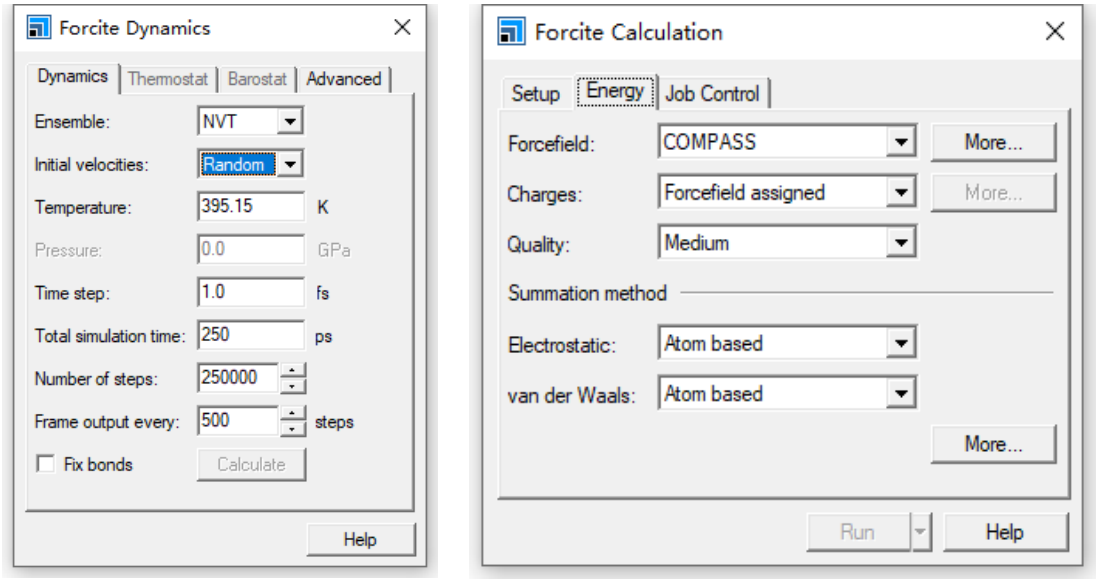


Figure 7. Parameter settings of molecular dynamics simulation.

3. Simulation Results and Analysis

3.1. Thermal Conductivity Calculation

The impact of nanoparticle size, mass concentration, and system temperature on the thermal properties of nano-fuel was investigated by analyzing thermal conductivity, heat flux distribution, and temperature gradients. Figure 8 shows the C14 fluid model constructed using the construction module in the Amorphous Cell (AC), comprising 1140 C14 molecules with a system density of 0.76 g/cm^3 and dimensions of 72 Å × 72 Å × 72 Å. Following its construction, the C14 fluid model underwent structural optimization and annealing using the Forcite module, with parameter settings identical to those used for the CeO_2 nano-fuel system.

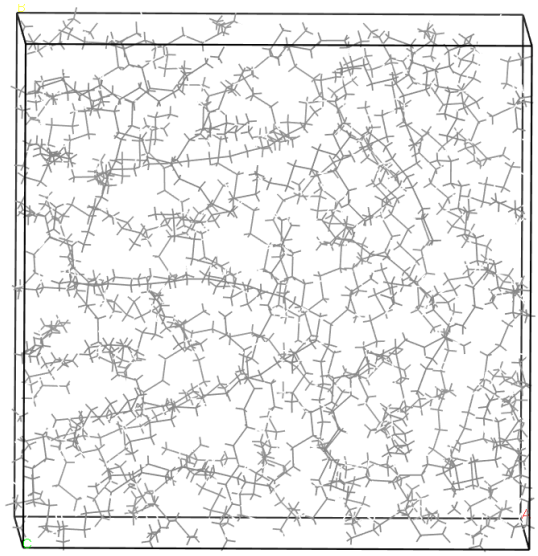


Figure 8. Construction of the C14 fluid model.

After completing structural optimization and annealing, a Perl script was developed to calculate the thermal conductivity of the C14 fluid. Along the *Z*-axis of the model, 20 layers were defined, with layers 0 and 19 designated as hot zones and layer 10 as the cold zone, forming a mirror-symmetric arrangement about layer 10. At a system temperature of 80 °C

under the NVT ensemble, the thermal conductivity of the C14 fluid was determined to be 0.1229 W/(m·K). The variation in the C14 fluid's thermal conductivity over simulation time is shown in Figure 9. The random motion of nanoparticles is a key factor influencing energy transfer within nano-fuels, while system temperature directly affects the intensity of such micro-movements. As can be seen from Figure 9, the thermal conductivity of Ce_{50}^{50} nano-fuel is closely related to temperature, and the thermal conductivity increases with the increase in system temperature. The thermal conductivity of Ce_{50}^{50} nano-fuel at different temperatures is shown in Table 3, from which it can be seen that when the system temperature is 60 °C and 100 °C, respectively, the thermal conductivity of Ce_{50}^{50} nano-fuel is 0.1440 W/(m·K) and 0.1622 W/(m·K), respectively. Compared with the thermal conductivity of Ce_{50}^{50} nano-fuel at 20 °C, it is increased by 9.8% and 23.6%, respectively.

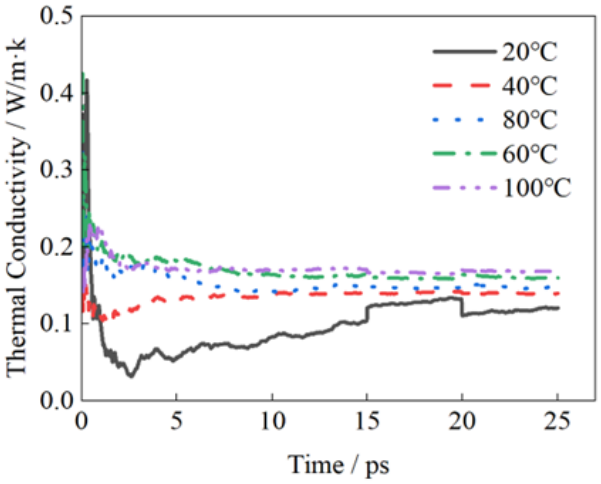


Figure 9. Thermal conductivity variation in the Ce_{50}^{50} nano-fuel.

Table 3. Thermal conductivity of Ce_{50}^{50} nano-fuel at various temperatures.

Temperature (°C)	Thermal Conductivity (W/(m·K))
20	0.1312
40	0.1386
60	0.1440
80	0.1547
100	0.1622

The growth rate of thermal conductivity accelerates with increasing system temperature due to enhanced nanoparticle movement and intensified interactions between nanoparticles and C14 molecules. Elevated system temperatures amplify the frequency of thermal exchanges between nanoparticles and the base fluid, thereby driving the observed increase in the thermal conductivity growth rate.

3.2. Radial Distribution Function

The radial distribution function (RDF) is a mathematical descriptor of the microstructure of atoms within a system, reflecting the aggregation characteristics of atoms. It quantifies the probability density of finding another type of atom within a spherical radius r centered on a given atom A. The schematic of RDF is shown in Figure 10, and its expression is as follows:

$$g_{\alpha\beta(r)} = \frac{V}{N_\alpha N_\beta}\left[\sum_{i=1}^{N\alpha}\frac{n_{i\beta}(r,\Delta r)}{4\pi r^2 \Delta r}\right] \quad (1)$$

where V denotes the volume (Å^3), N_α and N_β represent the number of atoms of each type, $n_{i\beta}(r, \Delta r)$ is the number of encounters between the two atom types, and Δr is the difference in particle radius. This study focuses on the RDF of atomic pairs within CeO_2 nano-fuel systems to investigate how nanoparticle size and mass concentration influence the microscopic mechanisms of base liquid fuel.

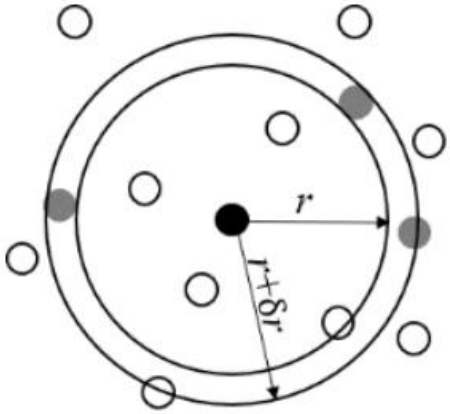


Figure 10. Schematic diagram of RDF.

3.2.1. Impact of Mass Concentration

In the CeO_2 nano-fuel system, the radial distribution function (RDF) module in Forcite was employed to analyze the RDFs of C-C, Ce-C, and Ce-Ce atomic pairs at varying nanoparticle mass concentrations.

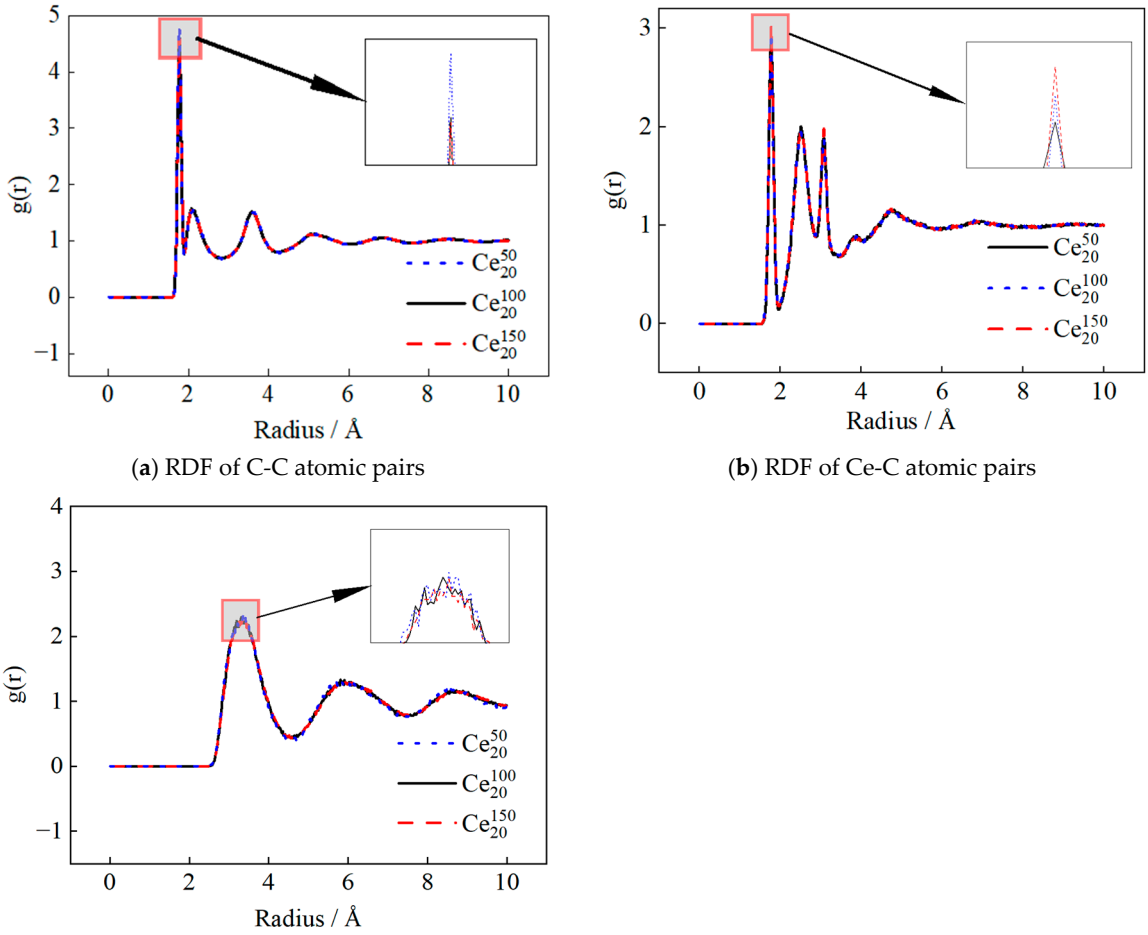
Figure 11a illustrates the RDFs of C-C atomic pairs in the Ce_{20} nano-fuel system under different mass concentrations. The RDF curves for C-C pairs in the Ce_{20} nano-fuel system show significant overlap across varying concentrations, reflecting the "short-range order, long-range disorder" microstructural characteristics of the base liquid fuel. This indicates that the mass concentration of nanoparticles has minimal impact on the probability of C-C atomic collisions. However, as the nanoparticle mass concentration decreases, the height of the first RDF peak gradually increases. This is attributed to the enlargement of the system size to maintain a constant nanoparticle diameter while reducing mass concentration, leading to the inclusion of more C14 molecules. Consequently, the probability of finding another C atom in close proximity slightly increases with the rise in C atom count.

Figure 11b depicts the RDF of Ce-C atomic pairs in the Ce_{20} nano-fuel system at different mass concentrations. The first peak of the RDF increases with rising mass concentration, contrary to the trend observed for C-C pairs. This suggests that, in the Ce_{20} nano-fuel system, a higher mass concentration increases the number of CeO_2 nanoparticles, thereby elevating the probability of Ce-C interactions. The increased interaction frequency enhances thermal exchange between Ce_{20} nanoparticles and C14 molecules, leading to an increase in the system's thermal conductivity.

Figure 11c shows the RDF of Ce-Ce atomic pairs in the Ce_{20} nano-fuel system at different mass concentrations. The RDF curve exhibits fewer peaks, with each peak's intensity decreasing with increasing distance. This indicates a high probability of Ce-Ce interactions. Interestingly, the nano-fuel with the highest first peak is Ce_{20}^{50}, while the first peak of Ce_{20}^{150}, the system with the highest mass concentration, is the lowest. This suggests that in Ce_{20} nano-fuel systems with lower mass concentrations, Ce-Ce interactions are more likely.

This phenomenon can be explained by the strong internal bonding and structural stability within CeO_2 nanoparticles, which resist deformation. At higher mass concentrations, the movement of Ce atoms within CeO_2 nanoparticles becomes restricted, reducing the

probability of Ce-Ce interactions within a given range. As the number of unattainable Ce atoms increases, the height of the first RDF peak decreases with increasing nanoparticle mass concentration.



(**a**) RDF of C-C atomic pairs

(**b**) RDF of Ce-C atomic pairs

(**c**) RDF of Ce-Ce atomic pairs

Figure 11. RDFs of Ce_{20} nano-fuels at different mass concentrations.

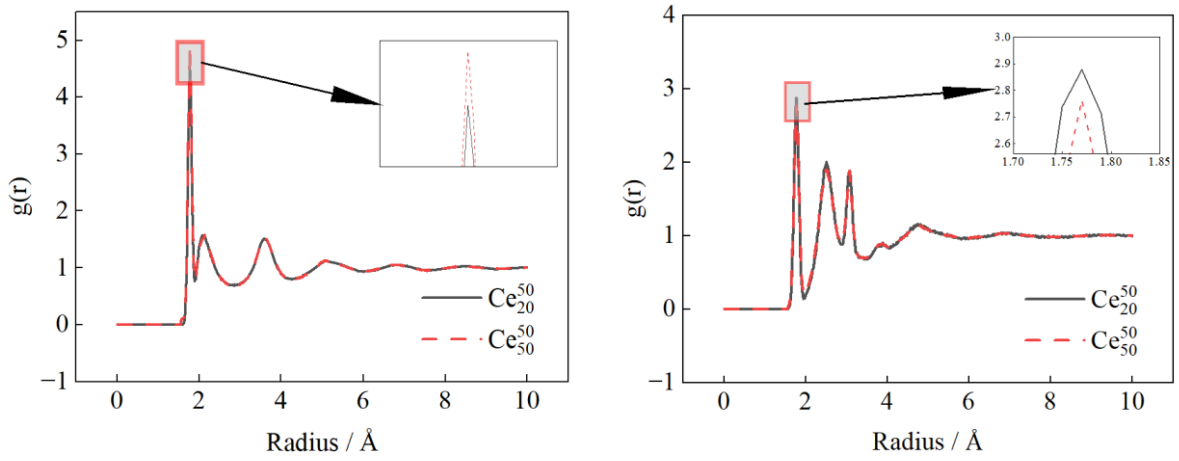
3.2.2. Effect of Nanoparticle Size

To elucidate the influence of nanoparticle size on nano-fuels, the radial distribution functions (RDFs) for C-C and Ce-C atomic pairs in the Ce^{50} nano-fuel system were analyzed at varying particle sizes. Figure 12a illustrates the RDF curves of C-C atomic pairs in the CeO_2 nano-fuel system under different nanoparticle sizes. Similarly to the findings in the previous section, the RDF of C-C pairs exhibits the characteristic "short-range order, long-range disorder" typical of base liquid fuel. The addition of nanoparticles alters the microstructure of the base liquid fuel. Notably, the first peak of the RDF is higher in the Ce_{50}^{50} nano-fuel system compared to the Ce_{20}^{50} system, indicating that as nanoparticle size increases, the likelihood of one C atom encountering another in the CeO_2 nano-fuel system rises.

This phenomenon can be attributed to the increase in system size to maintain a constant mass concentration of CeO_2 nanoparticles as their size grows, thereby incorporating more C14 molecules. Consequently, the number of C atoms rises with increasing nanoparticle size, enhancing the probability of one C atom encountering another in close proximity.

Figure 12b presents the RDF curves of Ce-C atomic pairs in the Ce^{50} nano-fuel system under varying nanoparticle sizes. The results reveal that as the size of CeO_2 nanoparticles increases, the number of nearby C atoms in the fuel decreases, leading to a lower

probability of Ce atoms encountering C atoms. This trend suggests that with larger CeO_2 nanoparticles, the frequency of Ce-C interactions diminishes, resulting in reduced thermal exchange between Ce_{20} nanoparticles and C14 molecules. Consequently, the capacity of CeO_2 nanoparticles to enhance heat transfer within the base liquid fuel diminishes, leading to a corresponding decrease in the system's thermal conductivity.



(**a**) RDF of C-C atomic pairs (**b**) RDF of Ce-C atomic pairs

Figure 12. RDFs of Ce^{50} nano-fuels at different particle sizes.

3.3. Diffusion Coefficient

Molecular diffusion refers to the migration of molecular structure caused by thermal movement of molecules in a system under the action of concentration difference or other driving force, which is a basic way of mass and energy transfer. In molecular dynamics, diffusion coefficients are primarily derived through mean square displacement (MSD) analysis. The quantitative relationship between MSD and the diffusion coefficient is established via Einstein's equation. The MSD can be expressed as [34–36] follows:

$$MSD_{(t)} = \left\langle \frac{1}{N}\sum_{i=1}^{N}|r_i(t) - r_i(0)|^2 \right\rangle \quad (2)$$

where $r_i(t)$ and $r_i(0)$ represent the positions of molecule i at time t and at the initial moment, respectively, and N is the number of molecules.

3.3.1. Effect of Mass Concentration

Figure 13 shows the MSD curves of C14 molecules in the Ce_{20} nano-fuel system at various temperatures. The simulation results indicate that the slope of the MSD curves increases with rising temperature, signifying greater molecular movement. A higher slope corresponds to a larger molecular displacement, reflecting more pronounced thermal motion. A comparison of Figure 13a–d reveals that, at the same temperature, the displacement of C14 molecules in the nano-fuel system exceeds that in the pure C14 fluid system. Moreover, the slope of the MSD curves becomes steeper as the mass concentration of nanoparticles increases, indicating greater molecular displacement per unit time and more intense thermal motion. Consequently, nano-fuels with higher mass concentrations exhibit greater thermal conductivity.

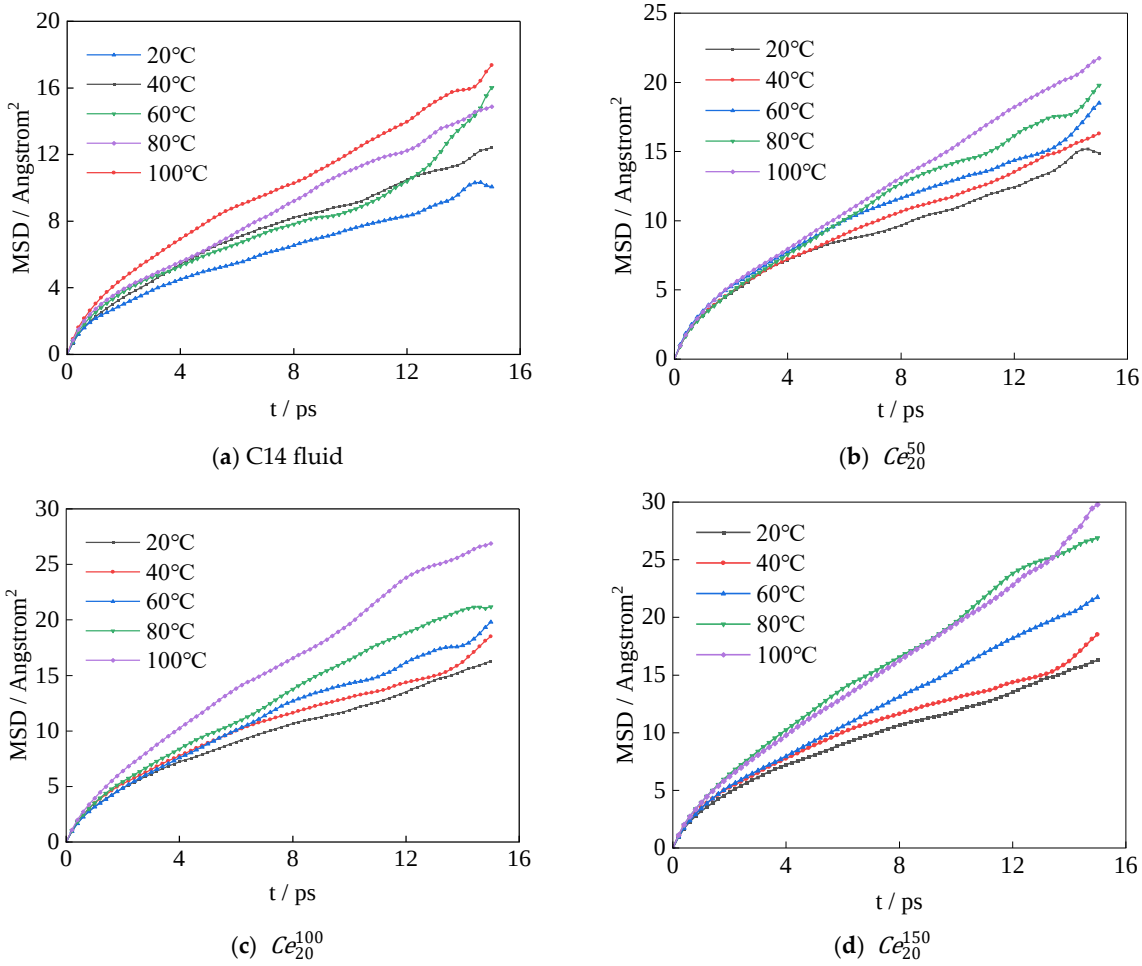


Figure 13. MSD characteristics of Ce_{20} nano-fuels under different temperatures.

The diffusion coefficient D is expressed as follows:

$$D = \lim_{t \to \infty} \frac{1}{6t} \langle |r_i(t) - r_i(0)|^2 \rangle \tag{3}$$

Combining Equations (2) and (3), the relationship between D and MSD is

$$D = \frac{MSD(t)}{6} \tag{4}$$

Table 4 presents the diffusion coefficients of Ce_{20} nano-fuel at different mass concentrations. The data demonstrate that, across all temperatures, the diffusion coefficient of Ce_{20} nano-fuel increases with higher nanoparticle mass concentrations. At 20 °C, increasing the mass concentration from 50 mg/L to 100 mg/L results in a 22% increase in the diffusion coefficient of C14 molecules. Further increasing the concentration from 100 mg/L to 150 mg/L yields a 14% increase.

This enhancement is attributed to the high specific surface area and surface activity of CeO_2 nanoparticles, which elevate the kinetic energy of C14 molecules adsorbed onto their surfaces. However, as the mass concentration continues to rise, the rate of increase in the diffusion coefficient diminishes, indicating an upper limit to the enhancement effect of nanoparticles on the diffusion coefficient of C14 molecules. This suggests that nanoparticles cannot infinitely augment the diffusion coefficient.

Table 4. Diffusion coefficients of Ce_{20} nano-fuels at different mass concentrations.

Mass Concentration (mg/L)	Temperature (°C)	Diffusion Coefficient (10^{-4} cm^2/s)
0	20	0.1139
	60	0.1411
	100	0.1778
50	20	0.1211
	60	0.1954
	100	0.2912
100	20	0.1451
	60	0.2663
	100	0.3602
150	20	0.1677
	60	0.3317
	100	0.4602

3.3.2. Effect of Temperature

Table 5 presents the diffusion coefficients of Ce_{20} nano-fuel across a temperature range of 20–100 °C. At 20 °C, the diffusion coefficient of Ce_{20}^{50} nano-fuel is 0.1211 × 10^{-4} cm^2/s. As the system temperature increases, the diffusion coefficient rises progressively. At 60 °C, the diffusion coefficient reaches 0.1954 × 10^{-4} cm^2/s, representing a 61.4% increase compared to its value at 20 °C. At 100 °C, the diffusion coefficient further increases to 0.2912 × 10^{-4} cm^2/s, marking a 140.05% enhancement relative to 20 °C.

Table 5. Diffusion coefficients of Ce_{20} nano-fuels at different temperatures.

Temperature (°C)	Mass Concentration (mg/L)	Diffusion Coefficient (10^{-4} cm^2/s)
20	0	0.1139
	50	0.1211
	150	0.1677
40	0	0.1231
	50	0.1624
	150	0.2468
60	0	0.1411
	50	0.1954
	150	0.3317
80	0	0.1591
	50	0.2418
	150	0.3865
100	0	0.1778
	50	0.2912
	150	0.4602

This temperature-dependent growth in the diffusion coefficient is attributed to the heightened activity and nanoscale effects of CeO_2 nanoparticles at elevated temperatures. The intensified thermal motion of both CeO_2 and C14 molecules leads to greater molecular displacement per unit time, thereby significantly enhancing the diffusion coefficient.

4. Conclusions

This study employed molecular dynamics simulations to explore the effects of CeO_2 nanoparticles on the heat transfer and flow properties of base liquid fuel. The key findings are summarized as follows:

First, the mass concentration of CeO_2 nanoparticles exhibits a strong correlation with the thermal conductivity of the nano-fuel. As the mass concentration increases, the

frequency of interactions between Ce and C atoms rises, leading to enhanced thermal exchanges and a notable improvement in the nano-fuel's thermal conductivity. System temperature also plays a significant role in boosting the thermal conductivity of CeO_2 nano-fuel. Elevated temperatures intensify internal heat transfer processes, resulting in a continuous increase in thermal conductivity with rising temperature.

Second, the addition of CeO_2 nanoparticles alters the microstructural behavior of the base liquid fuel (C14). The radial distribution function (RDF) curves of CeO_2 nano-fuel reveal a combination of the "short-range order, long-range disorder" typical of the base liquid fuel and the "long-range order" characteristic of nanoparticles.

Moreover, the diffusion coefficient of C14 increases with higher mass concentrations of CeO_2 nanoparticles. However, as the mass concentration increases further, stronger nanoparticle aggregation weakens the nanoscale effects of CeO_2 nanoparticles, partially limiting the enhancement of C14 diffusion. This suggests an upper limit to the ability of nanoparticles to further improve the diffusion coefficient of the base liquid fuel. Additionally, system temperatures directly influence the diffusion coefficient, with higher temperatures stimulating molecular thermal motion, leading to an increase in the diffusion coefficient of C14.

Author Contributions: Conceptualization, R.Z. and J.Z.; data curation, R.Z. and J.Z.; formal analysis, W.X.; funding acquisition, R.Z.; investigation, W.X.; methodology, Y.Z. and Z.H.; visualization, Y.Z. and Z.H.; project administration, W.Z.; resources, W.X.; software, Y.Z. and Z.H.; supervision, W.Z.; validation, R.Z. and J.Z.; writing—original draft, R.Z. and J.Z.; writing—review and editing, R.Z. and W.Z. All authors have read and agreed to the published version of the manuscript.

Funding: This research was funded by the Hunan Provincial Natural Science Foundation (Grant No. 2024JJ8026) and Belt and Road Project in Jiangsu Province (Grant No. BZ2022016).

Data Availability Statement: The data that support the findings of this study are available from the corresponding author upon reasonable request.

Conflicts of Interest: The authors declare no conflicts of interest.

References

1. Nautiyal, P.; Subramanian, K.A.; Dastidar, M.G.; Kumar, A. Experimental assessment of performance, combustion and emissions of a compression ignition engine fueled with Spirulina platensis biodiesel. *Energy* **2020**, *193*, 116861. [CrossRef]
2. Chen, A.F.; Adzmi, M.A.; Adam, A.; Othman, M.F.; Kamaruzzaman, M.K.; Mrwan, A.G. Combustion characteristics, engine performances and emissions of a diesel engine using nanoparticle-diesel fuel blends with aluminium oxide, carbon nanotubes and silicon oxide. *Energy Convers. Manag.* **2018**, *171*, 461–477. [CrossRef]
3. Jiang, L.; Xie, X.; Wang, L.; Wang, R.Z.; Wang, Y.D.; Roskilly, A.P. Investigation on an innovative sorption system to reduce nitrogen oxides of diesel engine by using carbon nanoparticle. *Appl. Therm. Eng.* **2018**, *134*, 29–38. [CrossRef]
4. Antonov, D.V.; Kuznetsov, G.V.; Sazhin, S.S.; Strizhak, P.A. Puffing/micro-explosion in droplets of rapeseed oil with coal micro-particles and water. *Fuel* **2022**, *3*, 123009–123017. [CrossRef]
5. Yuan, Z.; Dai, Y.; Liu, J.; Li, K. Light-Fueled Self-Propulsion of Liquid Crystal Elastomer-Engined Automobiles in Zero-Energy Modes. *Mathematics* **2024**, *12*, 2109. [CrossRef]
6. Ashraf, M.Z.; Rehman, S.U.; Farid, S.; Hussein, A.K.; Ali, B.; Shah, N.A.; Weera, W. Insight into Significance of Bioconvection on MHD Tangent Hyperbolic Nanofluid Flow of Irregular Thickness across a Slender Elastic Surface. *Mathematics* **2022**, *10*, 2592. [CrossRef]
7. Alahmer, A.; Rezk, H.; Aladayleh, W.; Mostafa, A.O.; Abu-Zaid, M.; Alahmer, H.; Gomaa, M.R.; Alhussan, A.A.; Ghoniem, R.M. Modeling and Optimization of a Compression Ignition Engine Fueled with Biodiesel Blends for Performance Improvement. *Mathematics* **2022**, *10*, 420. [CrossRef]
8. Rimkus, A.; Žaglinskis, J. Study of the Combustion Characteristics of a Compression Ignition Engine Fueled with a Biogas–Hydrogen Mixture and Biodiesel. *J. Mar. Sci. Eng.* **2024**, *12*, 2192. [CrossRef]

9. Gao, Z.; Xiao, Y.; Mao, J.; Zhou, L.; Li, X.; Li, Z. Optimization of Second-Generation Biodiesel Blends to Enhance Diesel Engine Performance and Reduce Pollutant Emissions. *Energies* **2024**, *17*, 5829. [CrossRef]
10. Man, D.; Pytel, B. Effect of Ionic and Nonionic Compounds Structure on the Fluidity of Model Lipid Membranes: Computer Simulation and EPR Experiment. *Membranes* **2024**, *14*, 257. [CrossRef]
11. Yu, Q.; Li, C.; Peng, B.; Tang, H.; Yang, T.; Yu, Y.; Zhang, K.; Chen, Z. Research Progress and Outlook of Molecular Dynamics Simulation on Carbon Dioxide Applied for Methane Exploitation from Hydrates. *Molecules* **2024**, *29*, 5579. [CrossRef] [PubMed]
12. Chen, H.; Zhao, K.; Luo, L.; Ma, Z.; Hu, Z.; Li, X.; Qu, P.; Pei, Y.; An, Y.; Gao, Z. A Numerical Simulation of Mixture Formation in a Hydrogen Direct-Injection Internal Combustion Engine. *Appl. Sci.* **2024**, *14*, 11317. [CrossRef]
13. Fang, Z.; Song, X. The Effect of H_2O_2 Pretreatment on TiO_2-Supported Ruthenium Catalysts for the Gas Phase Catalytic Combustion of Dichloromethane (CH_2Cl_2). *Catalysts.* **2024**, *14*, 886. [CrossRef]
14. Van, K. *Stochastic Processes in Physics and Chemistry*; Elsevier: Amsterdam, The Netherlands, 1992.
15. Tian, L. *Molecular Dynamics Simulation of Thermal Conductivity of Nanofluids*; Yanshan University: Qinhuangdao, China, 2021.
16. Kumar, R.; Gupta, A. Role of Brownian motion on the thermal conductivity enhancement of nanofluids. *Appl. Phys. Lett.* **2007**, *91*, 223102–223123.
17. Yang, P. *Molecular Dynamics Simulation of Enhanced Heat Transfer and Flow Characteristics of Nanofluids*; Chongqing University: Chongqing, China, 2017.
18. Sundar, L.S.; Otero-Irurueta, G.; Singh, M.K.; Sousa, A.C. Heat transfer and friction factor of multi-walled carbon nanotubes–Fe_3O_4 nanocomposite nanofluids flow in a tube with/without longitudinal strip inserts. *Int. J. Heat Mass Transf.* **2016**, *100*, 691–703. [CrossRef]
19. Nasrin, R.; Rahim, N.A.; Fayaz, H.; Hasanuzzaman, M. Water/MWCNT nanofluid based cooling system of PVT: Experimental and numerical research. *Renew. Energy* **2018**, *121*, 286–300. [CrossRef]
20. Omid, M.; Lioua, K.; Mohammad, A.; Estellé, P.; Ahmadi, G.; Kleinstreuer, C.; Pop, I. Recent advances in modeling and simulation of nanofluid flows—Part II: Applications. *Phys. Rep.* **2019**, *791*, 1–59.
21. Mohammad, K.; Hossein, H. Lattice Boltzmann simulation of nanofluid free convection heat transfer in an L-shaped enclosure. *Superlattices Microstruct.* **2014**, *66*, 112–128.
22. Wei, M.; Song, Y.; Wang, Y. Heat transfer of nanofluidics in hydrophilic pores: Insights from molecule dynamics simulations. *Chin. J. Chem. Eng.* **2016**, *24*, 1117–1121. [CrossRef]
23. Zheng, L.; Zhao, Q.; Dong, Y.; Jin, H.; Bawaa, B.; Guo, L. Molecular dynamics simulation of sub- and supercritical water extraction shale oil in slit nanopores. *J. Supercrit. Fluids* **2023**, *195*, 105862.
24. Tang, X.; Xiao, S.; Lei, Q.; Yuan, L.; Peng, B.; He, L.; Luo, J.; Pei, Y. Molecular Dynamics Simulation of Surfactant Flooding Driven Oil-Detachment in Nano-Silica Channels. *J. Phys. Chem. B* **2019**, *123*, 277–288. [CrossRef]
25. Fu, T.; Mao, Y.; Tang, Y.; Zhang, Y.; Yuan, W. Effect of nanostructure on rapid boiling of water on a hot copper plate: A molecule dynamics study. *Heat Mass Transf.* **2016**, *52*, 1469–1478. [CrossRef]
26. Azimi, S.S.; Kalbasi, M. A molecule dynamics simulation of brownian motion of a nanoparticle in a nanofluid. *Nanoscale Microscale Thermophys. Eng.* **2017**, *21*, 263–277. [CrossRef]
27. Tyagi, H.; Phelan, P.E.; Prasher, R.; Peck, R.; Lee, T.; Pacheco, J.R.; Arentzen, P. Increased hot-plate ignition probability for nanoparticle-laden diesel fuel. *Nano Lett.* **2008**, *8*, 1410–1416. [CrossRef] [PubMed]
28. Han, W.; Dai, B.; Liu, J.; Sun, Y.; Zhu, B.; Liu, X. Ignition and combustion characteristics of heptane-based nanofluid fuel droplets. *Energy Fuels* **2019**, *33*, 10282–10289. [CrossRef]
29. Chen, W.; Zhu, B.; Sun, Y.; Guo, P.; Liu, J. Nano-sized copper oxide enhancing the combustion of aluminum/kerosene-based nanofluid fuel droplets. *Combust. Flame* **2022**, *240*, 112028. [CrossRef]
30. Bhuiyan, M.H.U.; Saidur, R.; Amalina, M.A.; Mostafizur, R.M.; Islam, A.K.M.S. Effect of nanoparticles concentration and their sizes on surface tension of nanofluids. *Procedia Eng.* **2015**, *105*, 431–437. [CrossRef]
31. Hu, M.Y.; Yin, K.; Wen, Y.F.; Song, S.; Xiong, Y.; Dai, Y.; Sun, L. Combining in-situ TEM observations and theoretical calculation for revealing the thermal stability of CeO_2 nanoflowers. *Nano Res.* **2022**, *15*, 1319–1326.
32. Wei, Y.Y.; Wang, X.Y.; Dong, L.H.; Liu, G.; Xia, Q.; Yuan, S. Molecule dynamics study on the effect of surfactant mixture on their packing states in mixed micelles. *Colloids Surf. A Physicochem. Eng. Asp.* **2021**, *43*, 11–20.
33. Muller-Plathe, F. A simple nonequilibrium molecule dynamics method for calculating the thermal conductivity. *J. Chem. Phys.* **1997**, *106*, 2878–2891. [CrossRef]
34. Zhao, Q.; Buens, S.E. Molecule dynamics simulation of secondary sorption behavior of montmorillonite modified by single chain quaternary ammonium cations. *Environ. Sci. Technol.* **2012**, *46*, 3999–4007. [CrossRef] [PubMed]

35. Xu, W.Y.; Qiu, X.; Xiao, S.; Hu, G.; Wang, F.; Yuan, J. Molecular dynamic investigations on the adhesion behaviors of asphalt mastic-aggregate interface. *Materials* **2020**, *13*, 5061–5071. [CrossRef]
36. Porath, L.; Derkaloustian, M.; Ewoldt, R.H.; Huang, J.; Ramlawi, N.; Evans, C.M. Relaxation of vitrimers with kinetically distinct mixed dynamic bonds. *Macromolecules* **2022**, *55*, 4450–4458. [CrossRef]

Disclaimer/Publisher's Note: The statements, opinions and data contained in all publications are solely those of the individual author(s) and contributor(s) and not of MDPI and/or the editor(s). MDPI and/or the editor(s) disclaim responsibility for any injury to people or property resulting from any ideas, methods, instructions or products referred to in the content.